Supplementary Material

1 Modeling of the rotating disks

The software MocKinG [1] was used to model a rotating, exponential disk for the stars and molecular gas. MocKinG was designed to fit kinematic models to velocity maps of high redshift galaxies by correcting for beam smearing effects. The PyMultiNest Nested Sampling Monte Carlo implementation [2] was used to perform the fitting and estimate errors.

All the model parameters were left free during the fitting process (PA, i, maximum velocity, radius of maximum velocity, and systemic velocity), except for the center of rotation which was fixed to the peak of continuum emission at 2.1 μm (Figure 1). The results of the modeling are shown in Supplementary Figures 2 and 3. While the velocity residuals of the stars appear to be uniform and do not show additional kinematic components, the velocity residuals of H_2 show non-circular motions that have been interpreted as inflows in the plane of the galaxy [3], and an additional kinematic component in the central < 30 pc in the structure identified as the torus. Signatures of rotation can be identified in the center, with blueshifts in the SE and redshifts in the NW as the velocities of the masers [4, 5]. For reference, we schematically indicate in Supplementary Figure 3 the orientation of the maser disk with a PA of 107°. As can be seen in this Figure, the PA of the molecular gas intriguingly approaches the orientation of the maser disk, although higher spatial resolution observations are needed to properly characterize the gas kinematics in the central < 30 pc of the galaxy.

2 Problems with a standard biconical model of radial outflow

Here we investigate the possibility that the velocity reversals observed in the velocity maps of the ionized gas (Figure 2) are the result of projection effects from a typical biconical radial outflow. We consider two possible scenarios: one in which the bicone axis is close to the plane of the sky (i.e., the inclination of the bicone axis is approximately 0°), and one in which the bicone axis is tilted by 15° from the plane of the sky (note that this corresponds also to the more general case where the inclination is between $\gtrsim 15°$ and $\lesssim 60°$). We do not consider the case of $i > 60°$, since this is inconsistent with the geometry of the ionization cone of the galaxy [3, 6], and the fact that NGC 4388 is a Seyfert 2 galaxy. In Supplementary Figure 4 we show a sketch of a bicone with the southern part tilted towards us as in NGC 4388. Note that it is a simple bicone model with uniform density and an azimuthally symmetric velocity law (constant outflow velocity, or the gas is first accelerating and then decelerating at the same radial distance from the nucleus). In addition, we focus only on the cone to the south since a significant part of the outflow to the north is hidden by the plane of the galaxy at these scales (Figure 1).

In the first scenario, a cone axis close to the plane of the sky, we would expect to see only the blueshifted material in the wall of the cone that is in front of the plane of the sky. If the cone is hollow and optically thin, it would be possible to see the redshifted and blueshifted material of the two walls of the cone. However, this would imply emission lines with double peaks, and those spectral profiles are not present in our data (see Supplementary Figure 1). In addition, the magnitude of the blueshifted and redshifted velocities should reach the same value at the same distance from the nucleus. In NGC 4388 the redshifted velocities to the southeast and the blueshifted velocities to the southwest reach the same maximum velocity at different radial distances from the nucleus. These remarkable changes in velocity are consistent with the patterns expected from precession around the cone axis [7, 8].

If the southern cone is tilted towards us and the opening angle is $\gtrsim 40°$ we could see directly the redshifted velocities from the lower end of the cone (Supplementary Figure 4). This orientation of a wide angle cone is, however, inconsistent with the symmetry observed in the outflow of [Si VI] in NGC 4388. First, in this scenario, the redshifted material should be observed at larger radii than the blueshifted material, which should be located closer to the nucleus. In NGC 4388 we observe the opposite. Second, the blueshifted velocities will always have a higher magnitude since they are located in the front part of the cone near the line-of-sight, and the redshifted velocities are located in the back side of the cone which is closer to the plane of the sky. As can be seen in Figure 2, the velocity shifts in NGC 4388 are fairly symmetric and the maximum velocity in these two regions is comparable (~ 180 km s^{-1}).

3 Modeling of the helical outflow

We created a kinematic model of a helical outflow to reproduce the symmetry and trajectory of the velocity reversals observed in the velocity maps of the ionized gas (Figure 2). The model is based on the assumption of material moving in a helical trajectory with constant velocity, as can be seen in Supplementary Figure 5. The geometry of the conical helix can be expressed by the following set of parametric equations and transformations:

$$z(t) = t$$
$$x(t) = tr\cos at$$
$$y(t) = tr\sin at$$

where t is a geometric parameter that represents position at a given time, a is the angular frequency, h is the height, and r is the radius of the helix. Then two transformation angles, Φ_o, the tilt angle above the plane, and α_o, the angle along the plane from a reference zero direction, can be calculated, together with the opening angle Θ and the vector distance to the origin d:

$$\Phi_o = \arctan\frac{z}{\sqrt{x^2+y^2}}$$
$$\alpha_o = \arctan\frac{y}{x}$$
$$\Theta = \arctan\frac{r}{h}$$
$$d = \sqrt{x^2+y^2+z^2}$$

which can be used to transform the coordinates in terms of the position angle α and inclination Φ,

$$z = d\sin(\Phi_o + \Phi)$$
$$y = d\cos(\Phi_o + \Phi)\sin(\alpha_o + \alpha)$$
$$x = d\cos(\Phi_o + \Phi)\cos(\alpha_o + \alpha)$$

The model was created in Python, using Astropy to handle the data cube, and the Numpy module to handle the various manipulations. A coordinate system based on the number of pixels in the data cube was used with the $xy-$plane representing the plane of the sky and the $z-$axis the line-of-sight. The three-dimensional model was projected onto an empty array of appropriate scale, by mapping the x and y coordinates of each point in the model onto the corresponding point on the array. Similarly, each point of the two-dimensional array was filled with the magnitude of the component of the velocity vector in the line-of-sight at that point of the three-dimensional helix, as can be seen in the left panel of Figure 4.

Once the model was created, it was fit to the velocity map of [Si VI] shown in Figure 4. In this map, we excluded data points with velocity dispersion values < 270 km s^{-1}. Physically, this mask reflects the higher velocity dispersion expected to be associated with the outflow. The specific threshold used matches the minimum required value to remove knots of gas in the plane of the galaxy that are not associated with the outflow while preserving as many of the valid pixels as possible. The fitting procedure was performed in Python, using the lmfit module to conduct a least-squares minimization between the model and the masked data. The helix was forced to originate at the AGN, as determined by the location of the peak of emission at 2.1 μm (Figure 1). Therefore, the model has four free parameters: the velocity of the outflow $v_{\rm out}$, the precession angle or opening angle Θ, the position angle of the major axis of the helix α, and the inclination Φ. Uncertainties in the best-fitting parameters were automatically generated using the lmfit package in Python.

An overlay of the best-fit model on the velocity map of [Si VI] is shown in Figure 4 (note that this is not a pixel-by-pixel fit). As can be seen in this Figure, we were able to reproduce the symmetry and trajectory of the velocity reversals observed in the velocity map of [Si VI] with the following parameters: a velocity $v_{\rm out} = 177.3 \pm 18.7$ km s^{-1}, a precession angle $\Theta = 40.5° \pm 5.5°$, a position angle of the major axis of the helix $\alpha = 205.4° \pm 12.3°$, and an inclination $\Phi = 5.7° \pm 2.3°$.

4 Possible precession mechanisms

Following [9] and [10], we consider three possible mechanisms that can lead to warping and precession of an accretion disk: radiation-driven instabilities, frame dragging (also known as Lense–Thirring precession), and torques induced from a SMBHB on a circumbinary disk. The first two mechanisms are discussed based on the assumption that the central object surrounded by the warped accretion disk is a single SMBH. Other known mechanisms such as magnetically-driven instabilities or anisotropic accretion events (e.g., an interaction with a nuclear star cluster) are not discussed here because the induced precession periods are usually longer than 10^7 years [9, 10], their exact geometry is unknown, and in the case of random accretion events, one would expect rather sudden changes in the outflow direction rather than a smooth precession [10].

Radiation produced by an accreting SMBH can modify the dynamics of an accretion disk. If the disk is warped and optically thick, the radiation pressure will produce nonaxisymmetric torques that will change the initial orientation of the disk. Two aspects of the radiation-driven instabilities make this process less likely to be the cause of the outflow precession in NGC 4388. First, the critical radius at which the disk becomes unstable ($R_{cr} = (5\pi)^2(\eta/\epsilon)^2 R_g$ in a radiation pressure dominated-disk, where η is the ratio between the vertical and the azimuthal viscosities in the disk usually $\eta \geq 10$ [9, 11], ϵ is the accretion efficiency usually 0.1, and R_g is the Schwarzschild radius of the SMBH) is larger than the outer radius of the maser disk $r \sim 0.3$ pc, suggesting that in this case, the disk is stable against radiation torques. Furthermore, the precession period (equation 16 in [9], see also [12]) is one to two orders of magnitude larger than the precession period of the helical outflow in NGC 4388 (1.6 Myr).

Frame dragging produced by a Kerr black hole causes precession of a disk if its orbital plane is inclined in relation to the equatorial plane of the black hole. The precession angular velocity $\Omega_{\rm LT}$ due to the Lense-Thirring effect is given by [13]: $\Omega_{\rm LT} = 2GJ_{\rm BH}/c^2r^3$ where G is the gravitational constant, c is the speed of light, r is the radial distance from the SMBH and $J_{\rm BH}$ is the angular momentum of the black hole, defined as $J_{\rm BH} = sGM_{\rm BH}^2/c$. The parameters $M_{\rm BH}$ and s correspond to the black hole mass and spin, respectively. Assuming a warping radius of 0.01 pc, a black hole mass of 9×10^6 $M_\odot$ and a black hole spin parameter $s = 1$, the precession angular velocity is 1.42×10^{-7} rad yr^{-1}, which corresponds to a precession period of 4.4×10^7 yr. Note that if the radius is larger (which appears to be the case in NGC 4388 based on the size of the maser disk), or the spin parameter is < 1, the precession period would be also larger. A precession period of 10^7 yr is typical for the Lense-Thirring effect (or the related Bardeen–Petterson effect [14]) in SMBHs [9, 10, 15].

In a SMBH binary system, disk precession may be caused by a misalignment between the angular momentum of the disk and the binary total angular momentum (the tidal torques tend to align the circumbinary disk with the orbital plane). Following [12], the tidal precession angular velocity is given by: $\Omega_{\rm prec} = 0.75(a/r)^2 q_1 q_2 \Omega$, where a is the semi-major axis of the binary, r is the radius of the circumbinary disk, $q_1 = M_1/(M_1 + M_2)$ and $q_2 = M_2/(M_1 + M_2)$ are the mass ratio parameters, and $\Omega = \sqrt{GM_{\rm bin}/r^3}$ is the angular frequency of the mean motion of the circumbinary disk at r. Substituting the measured values for $M_{\rm bin} = 9 \times 10^6$ $M_\odot$ and $r = 0.3$ pc from the maser rotation curve, and assuming a mass ratio of $1:5$ between M_1 and M_2, a precession period of 1.6 Myr is obtained ($P_{\rm prec} = 1/\Omega_{\rm prec}$) for a binary separation of $a = 0.021$ pc. This is consistent with the values obtained from numerical simulations [12], which suggest that if the warping radius is of the order of 0.1 pc, a resultant semi-major axis is estimated to be of the order of 10^{-2} pc to 10^{-4} pc for a 10^7 $M_\odot$ SMBHB.

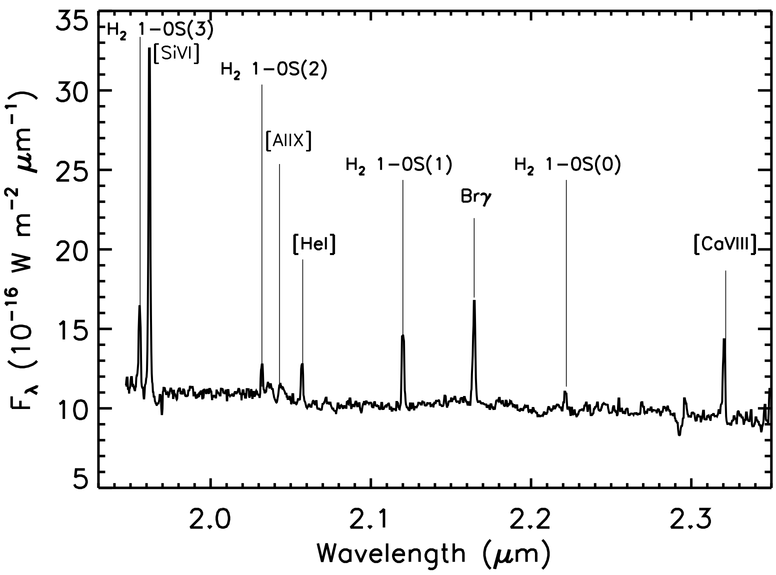

Supplementary Figure 1 $K-$band nuclear spectrum of NGC 4388 extracted in an aperture of $0.5''$ centered at the position of the AGN. Wavelengths are in the rest frame. The spectrum has been smoothed with a median filter of 3 pixels. All the emission lines detected are indicated with a solid line.

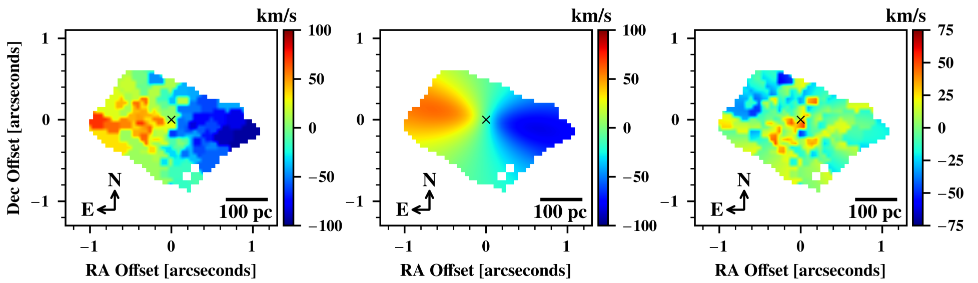

Supplementary Figure 2 Modeling of the stellar kinematics. From left to right: data, model, residuals. The cross indicates the position of the AGN in the three panels.

References

[1] Epinat, B., Amram, P., Balkowski, C., Marcelin, M.: Evidence for strong dynamical evolution in disc galaxies through the last 11 Gyr. GHASP VIII – a local reference sample of rotating disc galaxies for high-redshift studies. Monthly Notices of the Royal Astronomical Society **401**(4), 2113–2147 (2010)

[2] Buchner, J., Georgakakis, A., Nandra, K., Hsu, L., Rangel, C., Brightman, M.,

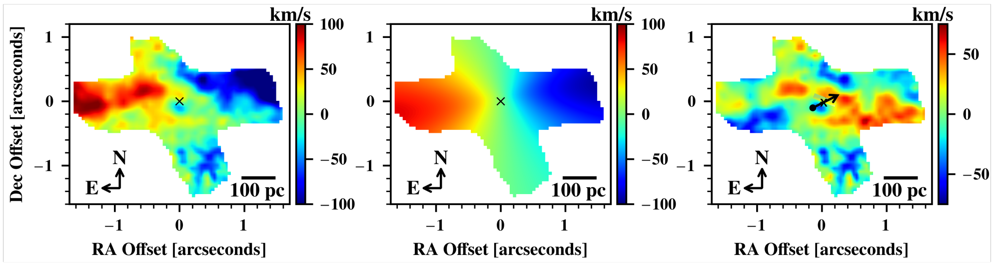

Supplementary Figure 3 Modeling of the molecular gas kinematics. From left to right: data, model, residuals. The cross indicates the position of the AGN in the three panels. The black arrow in the residuals map indicates the orientation of the maser disk (107°). The beginning of the arrow indicates the blueshifted velocities in the maser disk and the ending of the arrow the redshifted velocities.

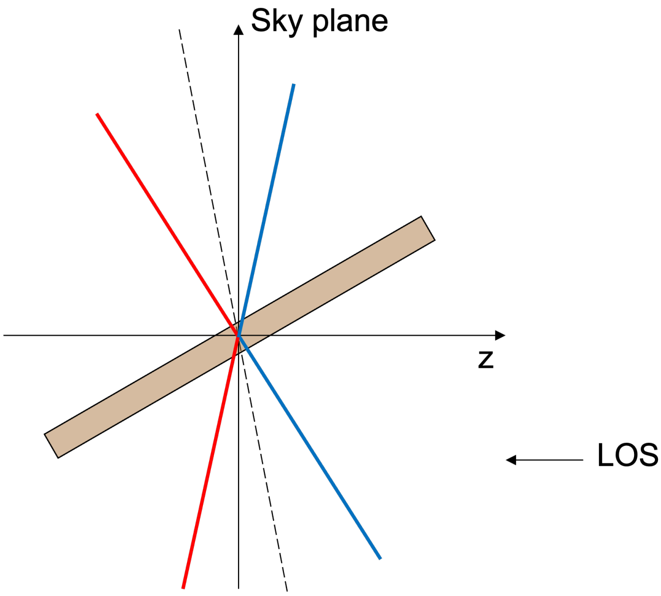

Supplementary Figure 4 Sketch of a hollow bicone with opening angle 40° and inclination angle 15° towards the observer in the south. The dashed line indicates the bicone axis. The brown rectangle represents the disk of the galaxy with the near side in the north as in NGC 4388. With a standard biconical model of radial outflow is impossible to reproduce the velocities of [Si VI].

Merloni, A., Salvato, M., Donley, J., Kocevski, D.: X-ray spectral modelling of the agn obscuring region in the cdfs: Bayesian model selection and catalogue. A&A **564**(1), 125 (2014)

[3] Greene, J.E., Seth, A., Lyubenova, M., Walsh, J., Ven, G., Läsker, R.: Circumnuclear molecular gas in megamaser disk galaxies ngc 4388 and ngc 1194. The Astrophysical Journal **788**(2), 145 (2014)

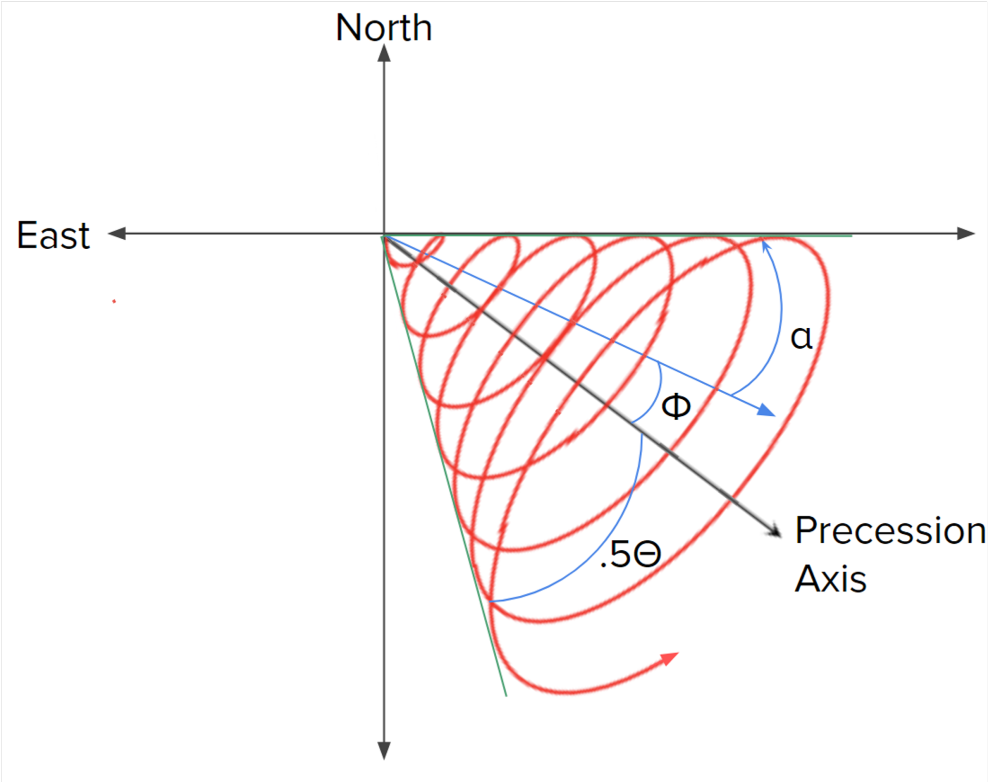

Supplementary Figure 5 Illustration of the helical outflow model in the reference frame of NGC 4388. The half-opening angle is 0.5Θ and the two angles referring to the orientation of the axis of the precessing conical helix are represented by α and Φ. The blue arrow indicates the projection of the precession axis in the plane of the sky.

[4] Braatz, J.A., Henkel, C., Greenhill, L.J., Moran, J.M., Wilson, A.S.: A green bank telescope search for water masers in nearby active galactic nuclei. The Astrophysical Journal **617**(1), 29 (2004)

[5] Kuo, C.Y., Braatz, J.A., Condon, J.J., Impellizzeri, C.M.V., Lo, K.Y., Zaw, I., Schenker, M., Henkel, C., Reid, M.J., Greene, J.E.: The megamaser cosmology project. iii. accurate masses of seven supermassive black holes in active galaxies with circumnuclear megamaser disks. The Astrophysical Journal **727**(1), 20 (2010)

[6] Falcke, H., Wilson, A.S., Simpson, C.: Hubble space telescope and vla observations of seyfert 2 galaxies: The relationship between radio ejecta and the narrow-line region*. The Astrophysical Journal **502**(1), 199 (1998)

[7] Rosen, A., Smith, M.D.: Hydrodynamic simulations of molecular outflows driven by fast-precessing protostellar jets. Monthly Notices of the Royal Astronomical

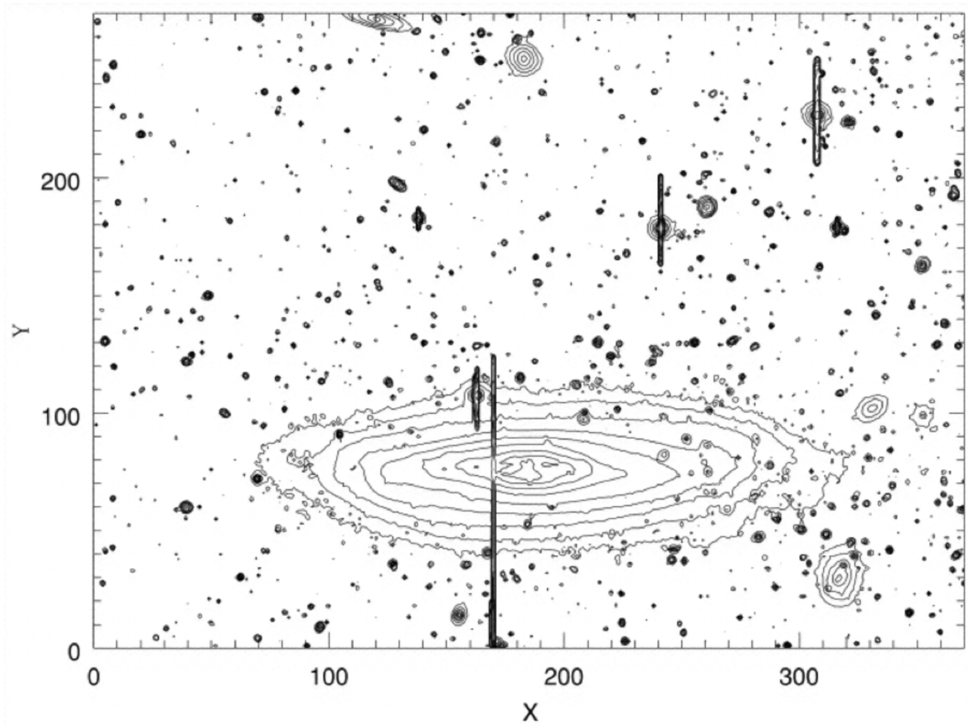

Supplementary Figure 6 Low surface brightness $R-$band image of NGC 4388. The shape of the bulge is boxy and a faint hump and tail are seen to the west of the galaxy. In addition, the outer isophotal contour is moderately asymmetrical with respect to the nucleus. All these morphological features indicate that NGC 4388 may be a minor merger remnant seen a few hundred Myr after the beginning of the merger event (image adapted from [16]).

Society **347**(4), 1097–1112 (2004)

[8] Aalto, S., Falstad, N., Muller, S., Wada, K., Gallagher, J. S., König, S., Sakamoto, K., Vlemmings, W., Ceccobello, C., Dasyra, K., Combes, F., García-Burillo, S., Oya, Y., Martín, S., van der Werf, P., Evans, A. S., Kotilainen, J.: Alma resolves the remarkable molecular jet and rotating wind in the extremely radio-quiet galaxy ngc 1377. A&A **640**, 104 (2020)

[9] Caproni, A., Livio, M., Abraham, Z., Cuesta, H.J.M.: Warping and precession in galactic and extragalactic accretion disks. The Astrophysical Journal **653**(1), 112 (2006)

[10] Krause, M.G.H., Shabala, S.S., Hardcastle, M.J., Bicknell, G.V., Böhringer, H., Chon, G., Nawaz, M.A., Sarzi, M., Wagner, A.Y.: How frequent are close supermassive binary black holes in powerful jet sources? Monthly Notices of the Royal Astronomical Society **482**(1), 240–261 (2018)

[11] Maloney, P.R., Begelman, M.C., Nowak, M.A.: Radiation-driven warping. ii. nonisothermal disks. The Astrophysical Journal **504**(1), 77 (1998)

[12] Hayasaki, K., Sohn, B.W., Okazaki, A.T., Jung, T., Zhao, G., Naito, T.: Warped circumbinary disks in active galactic nuclei. The Astrophysical Journal **790**(1), 62 (2014)

[13] Wilkins, D.C.: Bound geodesics in the kerr metric. Phys. Rev. D **5**, 814–822 (1972)

[14] Bardeen, J.M., Petterson, J.A.: The lense-thirring effect and accretion disks around kerr black holes. Astrophysical Journal Letters **195**(1), 65 (1975)

[15] Lodato, G., Pringle, J.E.: The evolution of misaligned accretion discs and spinning black holes. Monthly Notices of the Royal Astronomical Society **368**(3), 1196–1208 (2006)

[16] Yoshida, M., Yagi, M., Okamura, S., Aoki, K., Ohyama, Y., Komiyama, Y., Yasuda, N., Iye, M., Kashikawa, N., Doi, M., Furusawa, H., Hamabe, M., Kimura, M., Miyazaki, M., Miyazaki, S., Nakata, F., Ouchi, M., Sekiguchi, M., Shimasaku, K., Ohtani, H.: Discovery of a very extended emission-line region around the seyfert 2 galaxy ngc 4388*. The Astrophysical Journal **567**(1), 118 (2002)